Organic Electronics 130 (2024) 107074

Contents lists available at ScienceDirect

Organic Electronics

journal homepage: www.elsevier.com/locate/orgel

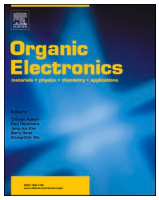

Tracking deep-level defects in degrading perovskite solar cells with a multifactorial approach

Carlos Biaou [a,*], Matthew Mcphail [b], Kazutaka Eriguchi [c], Vivek Subramanian [b,d], Oscar Dubon [a,c]

[a] Applied Science & Technology, University of California, CA, Berkeley, USA
[b] Electrical Engineering & Computer Science, University of California, CA, Berkeley, USA
[c] Materials Science & Engineering, University of California, CA, Berkeley, USA
[d] Microengineering, École Polytechnique Fédérale de Lausanne, Switzerland

ARTICLE INFO

Keywords:
Perovskite
Degradation
Photovoltaic
Multifactorial
PICTS
Deep-level traps

ABSTRACT

In this work, we provide a mechanistic understanding of the degradation of perovskite solar cells in operation by focusing on methylammonium lead triiodide ($CH_3NH_3PbI_3$ or $MAPbI_3$) and tracking the evolution of electronic defects via photo-induced current transient spectroscopy (PICTS). Moreover, we also record the degradation of its photovaltaic characteristics over time under various electric load and temperature conditions. Using PICTS, we found that bands of trap states, initially highly localized deep within the band gap of the perovskite, widened over the exposure period. This effect was exacerbated with increasing temperature. Further, using the design of experiment methodology for this multifactorial study, we found that two interaction factors (temperature× load & temperature× time) were significant in the degradation of the perovskite cells, validating the importance of our holistic approach. Through these observations, we establish a mechanistic link between deep-level traps and photovoltaic characteristics.

1. Introduction

In 2009, a perovskite solar cell delivering 3.8 % power conversion efficiency (PCE) was achieved [1]. Then, in 2012, a solution-processed perovskite solar cell with a PCE of 10.9 % was demonstrated [2]. Ever since, a race for the highest PCE perovskite solar cells has risen to prominence with the latest confirmed maximum PCE, as of 2024, at 26.1 % [3]. However, to be realistically viable [4], perovskites need to overcome the problem of long-term stability [5]. Numerous studies, both theoretical and experimental, have tackled the issue. Some studies have looked solely at the effects of humidity, temperature, or oxygen on the active layer [6], whereas others focused on the effects of UV light on the solar cell structure [7]. These single factor studies provide invaluable insights on the degradation of perovskites. Yet, a more holistic approach is needed to understand the effects of salient primary factors along with confounding higher order factors on the degradation. Few studies have employed a multifactorial approach in perovskite degradation investigations [8,9]. In this study, we implement the design of experiment (DOE) methodology, for it is uniquely suited for this endeavor. It provides a structured framework to simultaneously vary multiple inputs to understand their impact on the measured outputs. The relevance of factors and their interaction is carried out via a p-test, and the correlation between multiple responses can also be readily obtained. This methodology allows us to mechanistically tie the evolution of electronic defects in degrading perovskites with their electrical properties.

To measure these defects, we rely on photoinduced current transient spectroscopy (PICTS), for it is uniquely suited to measure deep-level traps in photosensitive devices with relatively high leakage currents like perovskites. It depends on transient currents generated from the device under testing (DUT) when excited by a pulsing light source and allows for the accurate extraction of the trap activation energy E_a —as low as 0.1 eV depending on the coolant [10]— and the capture cross-section σ_a. To perform such experiments, it is necessary to prime the traps repetitively, while the temperature is scanned, by pulsing photons of energy greater than the band gap. The excess electrons and holes are captured at trapping sites and subsequently released by thermal emission when the light is turned off, producing a current transient.

* Corresponding author.
E-mail address: cbiaou@berkeley.edu (C. Biaou).

https://doi.org/10.1016/j.orgel.2024.107074
Received 24 March 2024; Received in revised form 12 May 2024; Accepted 14 May 2024
Available online 16 May 2024

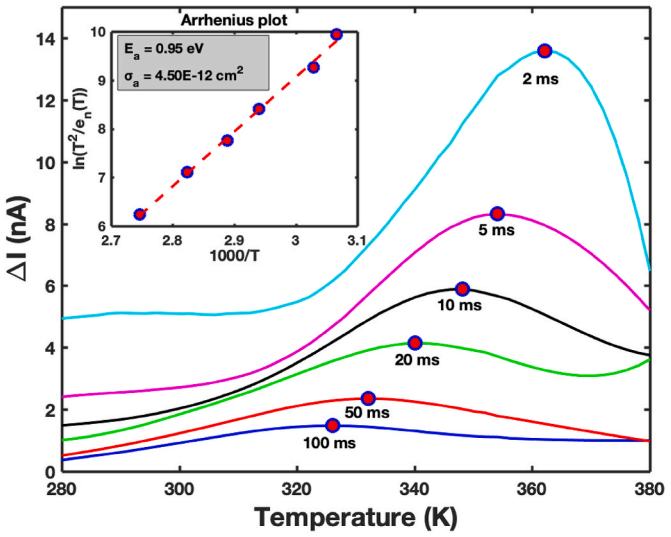

Fig. 1. PICTS Spectra of a fresh $MAPbI_3$ solar cell with a 1 ms filling pulse at 6 different rate windows (or delays). (**Inset**) Corresponding Arrhenius plot with extracted E_a and σ_a.

PICTS has previously been used to characterize GaAs substrates [11], CdTe [12], and perovskite solar cells [13,14].

Here, we provide a mechanistic understanding of the degradation of perovskite solar cells in operation by focusing on the evolution of deep-level traps (PICTS) in methylammonium lead triiodide ($CH_3NH_3PbI_3$ or $MAPbI_3$) and concurrently tracking its photovoltaic (IV) characteristics over time under various electrical load and temperature conditions. Using these observations, we will discuss avenues for improving the stability of metal halide perovskites.

2. Materials & methods

2.1. Experimental design

Our experimental design is an unreplicated $2^2 \times 5$ full factorial where the factors are temperature, electric load, and exposure period. For the temperature, we have chosen two levels, 25 °C and 55 °C, that respectively represent room temperature and roughly the highest ambient temperature recorded on Earth. For the electric load conditions, we also chose two levels, open-circuit (OC) and maximum power point (MPP) as they represent the most and least conservative degradation scenarios [8]. Exposure duration was the last factor, and the 5 periods chosen (0, 15, 45, 105, and 225 min) captured the full degradation of our unencapsulated $MAPbI_3$-based devices.

We tracked two broad categories of responses:

(1) the photovoltaic characteristics extracted from current-voltage curves —short-circuit current density (J_{SC}), the open-circuit voltage (V_{OC}), the fill factor (FF), and the power conversion efficiency (PCE);
(2) the deep level electronic defect properties (E_a & σ_a) evaluated using PICTS.

2.2. Sample preparation

FTO coated glass (7 Ω/sq, MSE supplies) was used as the substrate for the solar cells. The substrates were successively cleaned in baths of a 2 % mixture of Hellmanex (Sigma-Aldrich) in DI water, acetone, and isopropanol for 5 min each in a sonicator. Then, they were exposed for 3 min to an oxygen plasma (March Plasmod) prior to spinning the electron transport material (ETM). The ETM was prepared from a titanium isopropoxide solution (Solaronix) to form the compact TiO_2 layer and a colloidal dispersion of TiO_2 nanoparticles of <50 nm (Solaronix). The hole transport material (HTM) precursor was prepared in a nitrogen glovebox (<5 ppm H_2O/O_2) from a solution of spiro-OMeTAD (288 mg, Sigma-Aldrich) in anhydrous chlorobenzene (4 mL, Sigma-Aldrich) and doped with a 520 mg/mL solution of bis(trifluoromethane)sulfonimide lithium in acetonitrile (70 μL, Sigma-Aldrich) and 4-tert-Butylphenol (115.2 μL, Sigma-Aldrich). The solution was stirred at room temperature until it reached homogeneity and was stored in the glovebox. This sample preparation process was adapted from the authors' previous work [15].

2.3. Perovskite precursor preparation

The $MAPbI_3$ precursor was prepared in a nitrogen glovebox (<5 ppm

Table 1
Experimental space for this work. All degradation was done at < 5 % RH. The skipped experiments do not affect the significance of the results. The order presented here does not reflect the randomized data collection process and is only for the reader's convenience.

	Factors			Responses Photovoltaic				Traps	
Exp #	Temp (°C)	Load	Time (min)	V_{OC} (V)	J_{SC} (mA/cm²)	FF	PCE (%)	E_a (eV)	σ_a (cm²)
1	25	OC	0	0.87	−20.58	0.48	8.58	0.96	5.9E-12
2	25	OC	15	0.85	−18.65	0.35	5.61	0.73	2.3E-14
3	25	OC	45	0.82	−23.27	0.44	8.47	0.75	1.4E-12
4	25	OC	105	0.74	−14.99	0.30	3.35	0.60	2.2E-16
5	25	OC	225	0.69	−2.56	0.21	0.36	0.70	2.2E-12
6	25	MPP	0	0.80	−18.04	0.35	5.04	0.95	4.3E-09
7	25	MPP	15	–	–	–	–	–	–
8	25	MPP	45	0.91	−22.87	0.44	9.21	0.80	5.0E-11
9	25	MPP	105	0.77	−7.62	0.30	1.74	0.75	1.9E-09
10	25	MPP	225	0.64	−2.50	0.26	0.40	0.58	8.0E-16
11	55	OC	0	0.87	−20.58	0.48	8.58	0.96	5.9E-12
12	55	OC	15	0.76	−8.78	0.36	2.26	0.78	1.6E-07
13	55	OC	45	0.76	−17.05	0.26	3.34	0.72	3.7E-13
14	55	OC	105	0.39	−7.46	0.38	1.09	0.77	2.7E-08
15	55	OC	225	0.57	−4.67	0.29	0.76	0.27	2.3E-14
16	55	MPP	0	0.80	−18.04	0.35	5.04	0.95	4.3E-09
17	55	MPP	15	–	–	–	–	–	–
18	55	MPP	45	0.80	−15.38	0.34	4.19	0.84	3.9E-10
19	55	MPP	105	0.80	−7.02	0.23	1.32	0.51	1.3E-16
20	55	MPP	225	0.66	−9.12	0.20	1.21	0.50	1.2E-14

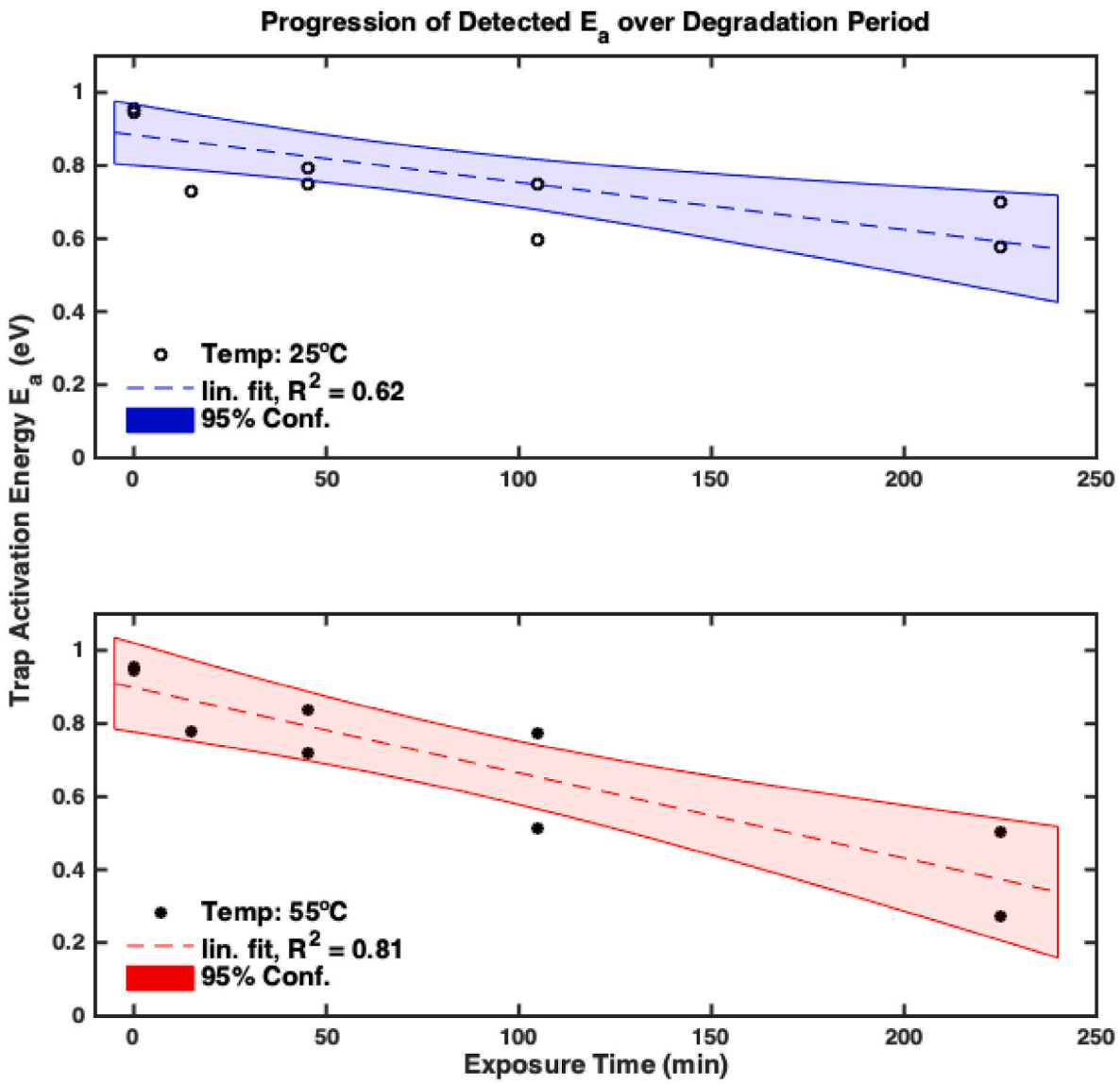

Fig. 2. Evolution of the trap activation energy over degradation time and temperature. The linear fits for the top and bottom plots are is $E_a = 0.88 - 1.3 \times 10^{-3}$ t and $E_a = 0.90 - 2.3 \times 10^{-3}$ t, respectively.

H_2O/O_2) from a solution of MAI (395 mg) and PbI_2 (1153 mg) in a 1:9 ratio of dimethylformamide (DMF, 2.25 mL) to dimethylsulfoxide (DMSO, 0.25 mL). The solution was stirred at room temperature until completely homogeneous and was stored in the glovebox. All reagents were purchased from Sigma-Aldrich. This precursor preparation process was adapted from the authors' previous work [15,16].

2.4. Solar cell fabrication

First, in a nitrogen glovebox, under low humidity conditions (<5 ppm H_2O/O_2), 100 μL of the titanium isopropoxide precursor was spun onto the FTO substrates at a speed of 5000 rpm and acceleration of 2000 rpm/s for 30 s. Then, they were dried at 150 °C for 10 min on a metal top hotplate followed by a sintering step under atmospheric conditions (70–80 % RH) at 500 °C for 30 min in a furnace to form the TiO_2 compact blocking layer. After the substrates cooled back down to room temperature under atmospheric conditions, the colloidal dispersion of TiO_2 nanoparticles was spun on top of the blocking layer at 5000 rpm and 2000 rpm/s for 30 s. They were subsequently dried at 150 °C for 2 min on a metal top hotplate followed by a sintering step at 475 °C for 30 min in a furnace to form the TiO_2 mesoporous layer. The substrates were moved to a nitrogen glovebox for the deposition of the perovskite layer. 100 µL of the perovskite precursor were spun under two consecutive regimes: regime 1 at 1000 rpm and 500 rpm/s for 10s and regime 2 at 6000 rpm and 3000 rpm/s for 25 s. Ten seconds into regime 2, droplets of cholorobenzene were deposited at a rate of 1 mL/min for a total volume of 100 µL using a digital syringe pump. Thereafter, the perovskite was annealed for 10 min at 100 °C on a metal top hotplate in the glovebox to form the active layer. Once cooled back down to room temperature, the HTM precursor was spun on top of the stack at 4000 rpm and 2000 rpm/s for 30 s. Finally, 80 nm of gold were thermally evaporated, using a stainless-steel mask, to form the top contact. The active area, defined as the overlap between the FTO and Au contacts, was 0.05 cm^2. This fabrication process was adapted from a published report [17].

2.5. Degradation set-up

An environmental chamber (AES BHD-503) was used in conjunction with a custom set-up made for this study. An incandescent light (150 W) was calibrated using a dimmer switch to deliver exactly 1 sun of irradiance to the DUT, which had a custom holder allowing for individual

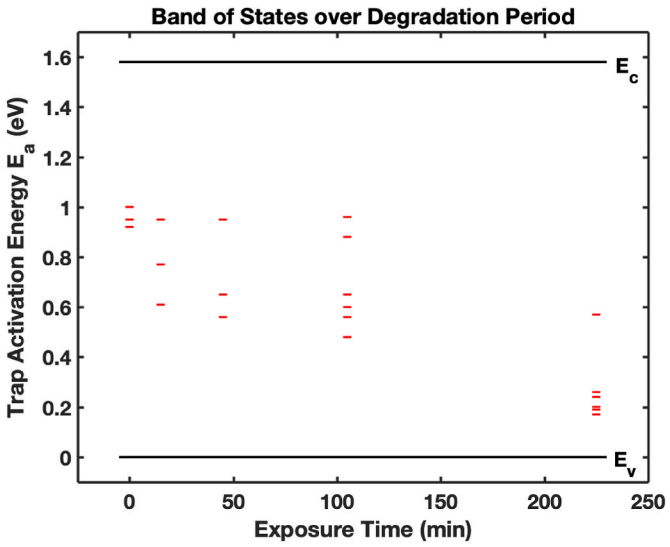

Fig. 3. Evolution of trap activation energy within the band gap of $MAPbI_3$ with filling pulses, at each degradation point, ranging from 1 to 1000 ms. Data extracted from Exp#11–15 of Table 1.

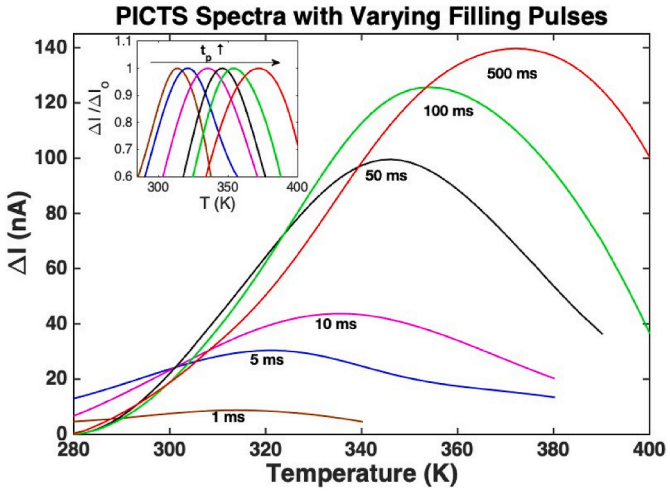

Fig. 4. PICTS Spectra of sample from Exp#14 in Table 1 with varying filling pulses t_p of period 2000 ms. (**Inset**) Normalized plot of the same spectra highlighting the right shift of the signal peak with increasing pulse width.

cells on a substrate to be connected to a 1 kΩ load (MPP) located outside the chamber. The holder consisted of a laser-cut piece of teflon with an opening in the center allowing light to penetrate the solar cells. Toothless copper alligator clips were attached to the teflon piece with aluminum wires, which doubled as leads to the electrical load. Teflon was chosen for its stability over the temperature and humidity ranges of the experiments. The toothless alligator clips were used to make direct contact with the gold anodes and the FTO cathode on the unencapsulated solar cells without significantly damaging them. Maintaining the load outside the chamber at atmospheric conditions ensured that the resistance was not varying over time. The PID controls of the environmental chamber were enabled to maintain constant temperature and humidity, especially when the incandescent light was on. This precursor preparation process was adapted from the authors' previous work [15, 16].

2.6. Measurements

Post-fabrication and pre-degradation, the photovoltaic characteristics of every cell were measured under atmospheric conditions. Then, post-exposure, those characteristics were measured once again and complemented by a PICTS measurement. The photovoltaic characteristics were measured using a solar simulator (Oriel-Sol1A) delivering an AM1.5 spectrum at 100 mW/cm^2 and a Keithley-2400. To collect the current-voltage data, a new MATLAB code from a previous report [18] was customized. The electronic defect data were obtained using a PICTS measurement system (Sula Technologies). The device was placed in a cryostat (Janis) and connected to the PICTS measurement set-up. Then, a LED of wavelength 626 nm was pulsed (2000 ms period) onto the device to generate carriers above the band gap of $MAPbI_3$ at 0 V bias. After evacuating the cryostat to below 10^{-5} Torr, the cold stage was cooled to 280K, the device temperature. The LabVIEW proprietary software controlling the set-up was programmed to record the spectrum of transient current at six different delays: 2, 5, 10, 20, 50 and 100 ms. As soon as the lower set temperature was reached, the system recorded data by progressively heating the device at a rate of 2K/min until it reached its ultimate temperature of 400K. The device was immediately returned to RT after the run was completed and never allowed to dwell too long at high or low temperatures. This process was repeated as the filling pulse was varied from 1 to 1000 ms for every sample to uncover the trapping dynamics of the defects. E_a and σ_a were extracted after each temperature spectral run via an Arrhenius plot.

3. Results

The data collected are summarized in Table 1.

3.1. Influence of degradation factors

To evaluate the importance of the degradation factors studied, we used p-tests of significance level $\alpha = 0.1$. The influence of temperature and electric load on the photovoltaic properties have been graphically reported in other studies [8]. However, we highlight the interaction terms that can only be revealed when performing degradation studies under a DOE framework. When considering the fill factor, we find that the interaction between temperature and electric load (pFF|Temp Load = 0.07) is relevant to its degradation, whereas the individual influence of temperature and electric load are not (pFF|Temp, Load >0.1). The other second order term deemed significant is the interaction of temperature with time for the trap activation energy—exposure time in this study should be understood as a confluence of atmospheric effects, illumination, and relative humidity (maintained at 5 % RH) because we did not vary them. The relevance of these interaction terms highlights the importance of undergoing degradation studies with a systematic and holistic approach to extract all the salient effects and make educated decisions. Any stability model should properly account for these interaction factors for accuracy.

3.2. Evolution of traps in degrading perovskites

Fig. 1 shows the PICTS spectra of a fresh (non-degraded) $MAPbI_3$ solar cell measured with a 1 ms filling pulse. Using 6 rate windows (or delays), we constructed the Arrhenius plot from the spectra's peaks revealing an activation energy $E_a = 0.95$ eV and capture cross-section $\sigma_a = 4.50\ 10^{-12}$ cm^2. This is a very deep trap, measured below the conduction band, for a solar cell whose absorber material band gap is 1.58 eV. After successfully characterizing this fresh sample, we measured the trap signatures of $MAPbI_3$ solar cells degraded in the conditions described in Table 1. For each condition, the reported E_a and σ_a was the average calculated from the filling pulses ranging from 1 to 1000 ms. Fig. 2 shows that the average trap activation energy gets shallower as the device is degraded over time. The shift is exacerbated by degradation at higher temperature, where the rate of degradation is almost doubled at 55 °C as compared to room temperature (25 °C). The capture cross-section generally follows the same trends as E_a. To better understand

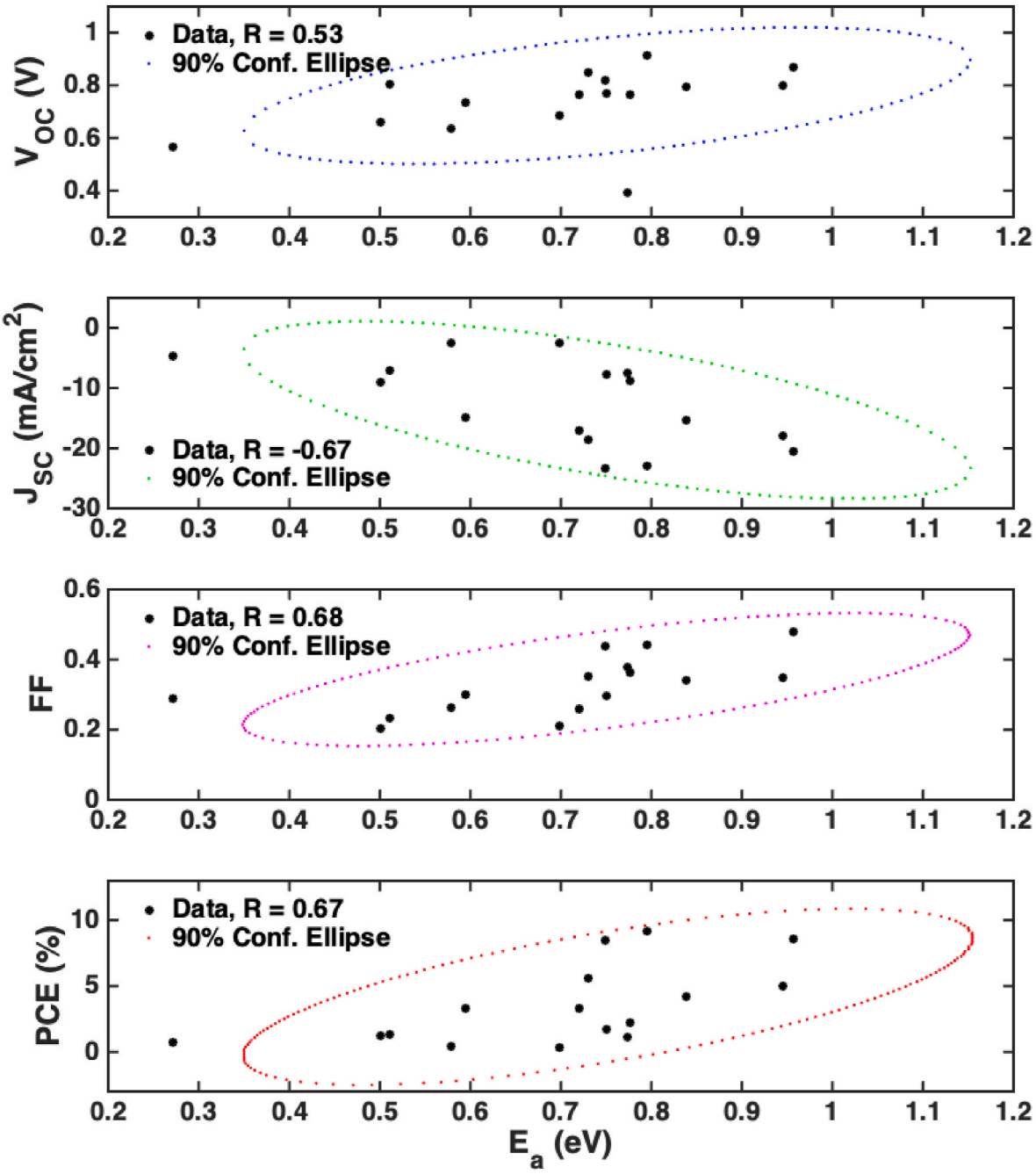

Fig. 5. (**From Top to Bottom**) Correlation plots of the open-circuit voltage, the short-circuit current, the fill factor and the power conversion efficiency as functions of the trap activation energy. The 90 % confidence ellipses of the dependent variables are included.

why the average E_a got closer to the conduction band, we focused on the bottom plot of Fig. 2 and plotted the raw activation energies instead of the averages. Fig. 3 shows a range of states widening over the degradation period. Two classifications of spatially extended defects in semiconductors were proposed: localized and band-like states [19]. This distinction lies in the comparison between the rate R_i at which the states reach their internal equilibrium and the emission (R_e) and capture (R_c) rates at which they reach equilibrium with the conduction band. In this theory, defect states are band-like if $R_i \gg R_c$, R_e and localized if $R_i \ll R_c$, R_e. Using simulated and measured deep level transient spectroscopy (DLTS) spectra, they showed that localized states had isothermal peaks, whereas band-like states had shifting emission peaks. As shown in Fig. 4, there is a general shift toward higher temperatures of the PICTS signal's peak as the filling pulse is increased. Consequently, we conclude that the degradation conditions of illumination and temperature interact synergistically to create spatially extended defects within the $MAPbI_3$ perovskite solar cells. These defects are characterized by band-like states since the PICTS spectra peaks shift with filling pulse. Prior to degradation, these states lie deep and narrow in the band gap with $0.92 \leq E_a \leq 1.0$ eV. By the end of the degradation period, they have widened to $0.17 \leq E_a \leq 0.57$ eV. It is very likely that we have not measured the complete range of the band-like states post-degradation since we limited our study to filling pulses of maximum width 1000 ms. Each trap may not have been completely filled with such pulses. This would explain why the range of the band-like states post-degradation does not fully overlap with the initial ones. We will tie this critical observation to physical mechanisms affecting the degradation of $MAPbI_3$ solar cells next.

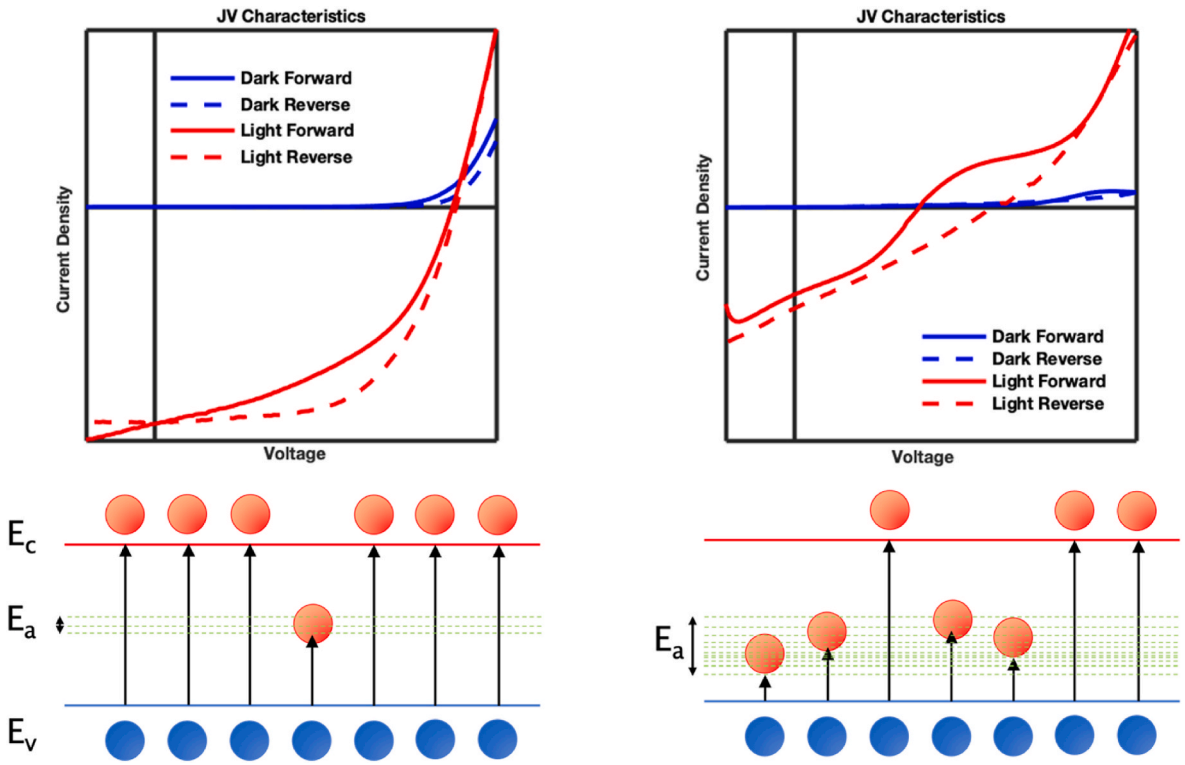

Fig. 6. Illustration of the trap mechanism affecting the photovoltaic characteristics of perovskites. (**Left**) Pre-degradation, carriers are easily promoted to the conduction band upon illumination since the traps are located deep within the band gap. The corresponding JV characteristic shows an ideal exponential behavior. (**Right**) Post-degradation, more carriers are captured due to the widened band of trap states resulting in loss of current and increased internal resistance characterized by the more linear JV curve.

3.3. Photovoltaic properties and deep-level traps

An examination of the correlation between the PV characteristics and the trap activation energy reveals that E_a's correlation to the PCE is mainly driven by a change in J_{SC} and FF and, to a lesser extent, a change in V_{OC} (See Fig. 5). Given that the short-circuit current is a measure of the number of photocarriers extracted from the solar cell, and the fill factor is one for the efficiency of that extraction, it is logical that they track well with the trap activation energy. Indeed, if the traps are initially located deep in the band gap, they are less likely to interfere with the photogeneration process. However, as discussed in Section 3.2, as the trap's band of states widens over the course of the degradation process, they are more likely to capture generated carriers, prevent them from reaching the conduction band, add to charge recombination, and decrease the output of useful current. This is akin to an internal resistance process, which would also explain the decrease in V_{OC} and FF (See Fig. 6).

4. Discussion

Our observations suggest that pinning traps deep within the perovskite's band gap is an essential key to unlocking their long-term stability. Indeed, extended traps impede full photon and photocarrier generation and collection. This process could be driven by the likely growth of crystallites within the perovskite in operando [20,21]. Preventing that crystallite growth is essential in extending the lifetime of perovskite solar cells, and we believe we can achieve it via two main methods. One would be to improve the formulation of the perovskite, especially at the A-site of its ABX_3 structure. Reducing the effective radius r_A of the A cation would shift the tolerance factor of the crystal structure toward the more desirable cubic lattice structure. It would also reduce the sensitivity of its crystal lattice to higher temperature, which is essential in promoting the crystallite's growth because heat is a significant driving factor. Optimizing r_A should be done by accounting for the narrow window in which functional and stable perovskite structures are expected to form. Indeed, a predictive probabilistic model has portrayed that critical window as a function of the cations' radii in the ABX_3 structure [22].

The other method for pinning the trap states would be by doping the perovskite. For instance, the incorporation of divalent ions such as alkaline earth metals Sr and Mg in limited amounts can increase the microstrain in the perovskite and reduce its crystallite size. It will also maintain its Goldschimdt tolerance factor t between 0.8 and 1.0, which is necessary for forming a 3D perovskite structure [23]. From DFT calculations, dopants could possibly substitute either the A or B cation in the ABX_3 or be incorporated interstitially [24]. The increased microstrain in the low doping regime showed an increase in V_{OC} and improved stability under light exposure in an inert environment. More systematic studies need to be undertaken to confirm these early predictions.

Beyond material selection and enhancement, the PICTS measurements outlined in this study, as it relates to perovskites specifically, could be most powerful as a manufacturing metrology for quality inspection on a sampling basis. Indeed, the deposition process used (CVD, blade coating, spin coating, etc.), the conditions of crystal growth and doping, temperature variations, impurities and mechanical stressors can all introduce or exacerbate defect states. Using a methodology similar to the one outlined in this study can provide standards for an acceptable level of defects in the manufactured cells and inform the quality of the fabrication process. This would be comparable to how light and elevated temperature induced degradation (LeTID) measurements are routinely performed in the Si solar cell industry to verify the batch-to-batch variation of manufactured solar cells and assess their susceptibility to boron and/or gallium doping induced LeTID.

5. Conclusions

In this article, we underwent a comprehensive multifactorial study of the degradation of perovskite solar cells in operation. We outlined the need for these multifactorial studies in the perovskite community and highlighted the benefits of this approach to improve cells toward the long-term stability standards necessary to making it a viable product. Our work confirmed the influence of interaction factors like temperature× load and temperature× time in the degradation of perovskite solar cells. These combinations of factors significantly alter the degradation rate when applied simultaneously and would have been missed in single-factor studies. We detailed how using PICTS helped us uncover that a band of trap states, initially narrowly constricted deep in the band gap of $MAPbI_3$, widened over the course of the degradation period, and that the average trap activation energy for each band of states became shallower. From our DOE analysis, we found that this effect was significantly correlated with the degradation of the other responses tracked in this study. We posited that the extension of the band of trap states over time, load, and temperature impeded the collection and generation of free carriers within the absorbing layer. We believe that process to be driven by the growth of crystallites. We thus concluded that pinning those traps deep within the band gap could unlock longer stability. Finally, we discussed improving the crystal structure to stabilize its crystallite growth by changing its constituent compounds or by doping. We also discussed using PICTS to assess the manufacturing quality of perovskite solar cells.

Funding

This material is based upon work supported by the National Science Foundation Graduate Research Fellowship under Grants No. DGE1106400 & DGE1752814, the Jack Kent Cooke Foundation, and the UC Berkeley Chancellor's Fellowship.

CRediT authorship contribution statement

Carlos Biaou: Writing – review & editing, Writing – original draft, Visualization, Validation, Software, Methodology, Investigation, Funding acquisition, Formal analysis, Data curation, Conceptualization. **Matthew Mcphail:** Methodology. **Kazutaka Eriguchi:** Methodology. **Vivek Subramanian:** Supervision, Project administration, Funding acquisition, Conceptualization. **Oscar Dubon:** Writing – review & editing, Supervision, Resources, Project administration, Methodology, Funding acquisition, Data curation, Conceptualization.

Declaration of competing interest

The authors declare that they have no known competing financial interests or personal relationships that could have appeared to influence the work reported in this paper.

Data availability

Data will be made available on request.

Acknowledgments

We acknowledge Lance Go and Matthew Anderson for the insightful conversations that helped mold this work. We also thank the staff of the Small Molecule X-ray Crystallography Facility and the Nanolab at Berkeley for their diligence. We recognize that this work was performed at UC Berkeley, which sits on the territory of Huichin, the ancestral and unceded land of the Chochenyo speaking Ohlone people, and that every member of the Berkeley community continues to benefit from the use and occupation of this land.

References

[1] A. Kojima, K. Teshima, Y. Shirai, T. Miyasaka, Organometal halide perovskites as visible-light sensitizers for photovoltaic cells, Journal of the American Chemical 131 (2009) 6050–6051, https://doi.org/10.1021/ja809598r.
[2] M.M. Lee, J. Teuscher, T. Miyasaka, T.N. Murakami, H.J. Snaith, Efficient hybrid solar cells based on meso-superstructured organometal halide perovskites, Science 338 (2012) 643–647, https://doi.org/10.1126/science.1228604.
[3] Best Research-Cell Efficiency Chart.URL https://www.nrel.gov/pv/assets/pdfs/best- research-cell-efficiencies.pdf.
[4] M. Cai, Y. Wu, H. Chen, X. Yang, Y. Qiang, L. Han, Cost-performance analysis of perovskite solar mod- ules, Adv. Sci. 4 (2017), https://doi.org/10.1002/advs.201600269, 1600269–1600269.
[5] M. Asghar, J. Zhang, H. Wang, P. Lund, Device sta- bility of perovskite solar cells - a review, Renew. Sustain. Energy Rev. 77 (2017) 131–146, https://doi.org/10.1016/j.rser.2017.04.003.
[6] Q. Dong, F. Liu, M.K. Wong, H.W. Tam, A.B. Djurišić, A. Ng, Encapsulation of perovskite solar cells for high humidity conditions, ChemSusChem 9 (2016) 2597–2603, https://doi.org/10.1016/j.rser.2017.04.003.
[7] W. Li, W. Zhang, S. Van Reenen, R.J. Sutton, J. Fan, A.A. Haghighirad, Enhanced uv-light stability of pla- nar heterojunction perovskite solar cells with caesium bromide interface modification, Energy Environ. Sci. 9 (2016) 490–498, https://doi.org/10.1039/C5EE03522H.
[8] K. Domanski, E.A. Alharbi, A. Hagfeldt, M. Grätzel, W. Tress, Systematic investigation of the impact of operation conditions on the degradation behaviour of perovskite solar cells, Nat. Energy 3 (2018) 61–67, https://doi.org/10.1038/s41560-017-0060-5.
[9] P. Tyagi, T.W. David, V.D. Stoichkov, J. Kettle, Multivariate approach for studying the degradation of perovskite solar cells, Sol. Energy 193 (2019) 12–19, https://doi.org/10.1016/j.solener.2019.09.054.
[10] M. Hage-Ali, B. Yaacoub, S. Mergui, M. Samimi, B. Biglari, P. Siffert, Microscopic defect level charac- terization of semi-insulating compound semiconduc- tors by tsc and picts: application to the effect of hydrogen in cdte, Appl. Surf. Sci. 50 (1991) 377–382, https://doi.org/10.1016/0169-4332(91)90202-U.
[11] M. Tapiero, N. Benjelloun, J.P. Zielinger, S.E. Hamd, C. Noguet, Photoinduced current transient spectroscopy in high-resistivity bulk materials: in- strumentation and methodology, Journal of Applied 64 (1988) 4006–4012, https://doi.org/10.1063/1.341361.
[12] X. Mathew, Photo-induced current transient spec- troscopic study of the traps in cdte, Solar En- ergy Materials and Solar Cells 76 (2001) 225–242, https://doi.org/10.1016/S0927-0248(02)00276-3.
[13] V. Pecunia, J. Zhao, C. Kim, B.R. Tuttle, J. Mei, F. Li, Y. Peng, T.N. Huq, R.L. Z. Hoye, N.D. Kelly, S.E. Dutton, K. Xia, J.L. MacManus- Driscoll, H. Sirringhaus, Assessing the impact of de- fects on lead-free perovskite-inspired photovoltaics via photoinduced current transient spectroscopy, Adv. Energy Mater. 11 (22) (2021) 2003968, https://doi.org/10.1002/aenm.202003968.
[14] G. Armaroli, L. Maserati, A. Ciavatti, P. Vecchi, A. Piccioni, M. Foschi, V.V. der Meer, C. Cortese, M. Feldman, V. Foderà, T. Lemercier, J. Zaccaro, J.M. Guillén, E. Gros-Daillon, B. Fraboni, D. Cav- alcoli, Photoinduced current transient spectroscopy on metal halide perovskites: electron trapping and ion drift, ACS Energy Lett. 8 (10) (2023) 4371–4379, https://doi.org/10.1021/acsenergylett.3c01429.
[15] C. Biaou, Towards a Better Mechanistic Understand- ing of the Degradation Processes of Perovskite Solar Cells (January 2018).URL https://www2.eecs.berkeley.edu/Pubs/TechRpts/2018/EECS-2018-3.pdf.
[16] C. Biaou, Multifactorial Investigation of Perovskite Solar Cell Degradation in Operation, This disserta- tion is under embargo until October 30, 2024 (De- cember 2020).URL https://escholarship.org/uc/item/5698r8c2.
[17] C. Yi, J. Luo, S. Meloni, A. Boziki, N. Ashari-Astani, C. Grätzel, Entropic stabilization of mixed a-cation abx3 metal halide perovskites for high performance perovskite solar cells, Energy Environ. Sci. 9 (2016) 656–662, https://doi.org/10.1039/C5EE03255E.
[18] E. Zimmermann, K.K. Wong, M. Müller, H. Hu, P. Ehrenreich, M. Kohlstädt, Characterization of perovskite solar cells: towards a reliable measure- ment protocol, Apl. Mater. 4 (2016), https://doi.org/10.1063/1.4960759, 91901–91901.
[19] W. Schröter, J. Kronewitz, U. Gnauert, F. Riedel, M. Seibt, Bandlike and localized states at extended defects in silicon, Phys. Rev. 52 (1995) 13726–13729, https://doi.org/10.1103/PhysRevB.52.13726.
[20] C.V. Thompson, R. Carel, Stress and grain growth in thin films, J. Mech. Phys. Solid. 44 (1996) 657–673, https://doi.org/10.1016/0022-5096(96)00022-1.
[21] C. Liu, Y.-B. Cheng, Z. Ge, Understanding of per- ovskite crystal growth and film formation in scalable deposition processes, Chem. Soc. Rev. 49 (6) (2020) 1653–1687, https://doi.org/10.1039/C9CS00711C.
[22] C.J. Bartel, C. Sutton, B.R. Goldsmith, R. Ouyang, C.B. Musgrave, L.M. Ghiringhelli, New toler- ance factor to predict the stability of perovskite oxides and halides, Sci. Adv. 5 (2019), https://doi.org/10.1126/sciadv.aav0693.
[23] V.M. Goldschmidt, Die Gesetze der Krystallo- chemie, Naturwissenschaften 14 (1926) 477–485, https://doi.org/10.1007/BF01507527.
[24] N. Phung, R. Félix, D. Meggiolaro, A. Al-Ashouri, G.S.E. Silva, C. Hartmann, The doping mechanism of halide perovskite unveiled by alkaline earth metals, Journal of the American Chemical 142 (2020) 2364–2374, https://doi.org/10.1021/jacs.9b11637.